Journal of Liposome Research

ISSN: (Print) (Online) Journal homepage: https://www.tandfonline.com/loi/ilpr20

AS1411aptamer conjugated liposomes for targeted delivery of arsenic trioxide in mouse xenograft model of melanoma cancer

Fatemeh Shariat Razavi, Maryam Kouchak, Neda Sistani Karampour, Masoud Mahdavinia, Zahra Nazari Khorasgani, Annahita Rezaie & Nadereh Rahbar

To cite this article: Fatemeh Shariat Razavi, Maryam Kouchak, Neda Sistani Karampour, Masoud Mahdavinia, Zahra Nazari Khorasgani, Annahita Rezaie & Nadereh Rahbar (16 Oct 2023): AS1411aptamer conjugated liposomes for targeted delivery of arsenic trioxide in mouse xenograft model of melanoma cancer, Journal of Liposome Research, DOI: 10.1080/08982104.2023.2271046

To link to this article: https://doi.org/10.1080/08982104.2023.2271046

JOURNAL OF LIPOSOME RESEARCH
https://doi.org/10.1080/08982104.2023.2271046

Taylor & Francis
Taylor & Francis Group

RESEARCH ARTICLE

AS1411aptamer conjugated liposomes for targeted delivery of arsenic trioxide in mouse xenograft model of melanoma cancer

Fatemeh Shariat Razavi[a,b], Maryam Kouchak[a,b], Neda Sistani Karampour[c,d], Masoud Mahdavinia[e,f], Zahra Nazari Khorasgani[f], Annahita Rezaie[g] and Nadereh Rahbar[a,h]

[a]Nanotechnology Research Center, Ahvaz Jundishapur University of Medical Sciences, Ahvaz, Iran; [b]Department of Pharmaceutics, School of Pharmacy, Ahvaz Jundishapur University of Medical Sciences, Ahvaz, Iran; [c]Marine Pharmaceutical Science Research Center, Ahvaz Jundishapur University of Medical Sciences, Ahvaz, Iran; [d]Department of Pharmacology, School of Pharmacy, Ahvaz Jundishapur University of Medical Sciences, Ahvaz, Iran; [e]Toxicology Research Center, Ahvaz Jundishapur University of Medical Sciences, Ahvaz, Iran; [f]Department of Toxicology, School of Pharmacy, Ahvaz Jundishapur University of Medical Sciences, Ahvaz, Iran; [g]Department of Pathobiology, Faculty of Veterinary Medicine, Shahid Chamran University of Ahvaz, Ahvaz, Iran; [h]Department of Medicinal Chemistry, School of Pharmacy, Ahvaz Jundishapur University of Medical Sciences, Ahvaz, Iran

ABSTRACT

Development of AS1411aptamer-conjugated liposomes for targeted delivery of arsenic trioxide is the primary goal of this study. AS1411aptamer was used as ligand to target nucleolin, which is highly expressed on the surface of melanoma cancer cells. The targeted liposomes were constructed by the thin film method, and arsenic trioxide was loaded as cobalt (II) hydrogen arsenite (CHA) to increase the loading efficiency and stability of the liposomes. The liposomal structure was characterized by Fourier Transform Infrared Spectroscopy (FT-IR) and field emission scanning electron microscopy (FESEM). In addition, particle sizes and zeta potential of the CHA-loaded liposomes (CHAL) and aptamer-functionalized CHA-loaded liposomes (AP-CHAL) were determined. *In vitro* cytotoxicity of CHAL and AP-CHAL were evaluated using MTT assay in murine melanoma (B16) and mouse embryonic fibroblast (MEF) cell lines. The encapsulation efficiency of CHAL and AP-CHAL was reported as 60.2 ± 6.5% and 58.7 ± 4.2%, respectively. *In vivo* antitumor activity of CHAL and AP-CHAL in the B16 tumor-xenograft mouse model was dramatically observed. All mice of both groups survived until the end of treatment and showed body weight gain. The tumor protrusion completely disappeared in 50% of the mice in these groups. Furthermore, histopathology studies demonstrated that CHAL and AP-CHAL did not induce significant toxicity in healthy mice tissues. However, unlike the CHAL group, which showed an initial increase in tumor volume, a specific antitumor effect was observed in the AP-CHAL group from the beginning of treatment. The results showed that AP-CHAL can be used as an effective drug delivery system with high potential in the treatment of solid tumors.

ARTICLE HISTORY
Received 5 May 2023
Revised 7 October 2023
Accepted 10 October 2023

KEYWORDS
Arsenic trioxide; functionalized liposomes; AS1411 aptamer; nucleolin; melanoma cancer

1. Introduction

Compounds containing the element arsenic (As), called arsenicals, have a long history of use in humans. Arsenic is one of the oldest drugs used to treat many disorders, such as rheumatism, anemia, malaria, and syphilis, in Western and traditional Chinese medicine [1–3]. In the early 1970s, arsenic trioxide (As_2O_3, ATO) was first used by the Chinese as an anti-cancer agent [3]. It has been approved by the FDA for the initial or recurrent treatment of acute promyelocytic leukemia (APL) since 2000 [4]. In addition, it has been shown that ATO induces apoptosis in cancer cells of the liver, brain, breast, prostate, kidney, bladder, and ovarian by reactive oxygen species [1,5]. Some other studies showed that ATO could promote differentiation, inhibit angiogenesis, and reduce the metastatic and invasive properties, as well as the migration of solid tumor cells [6–9]. However, the drug has not been very successful in clinical trials for the treatment of solid tumors due to its limitations, such as rapid renal clearance [10], high serum protein binding [1,7], and dose-limiting toxicity [11].

Nowadays, significant progress has been achieved in cancer therapy using nanotechnology. Liposomes are extensively used as a group of nanocarriers to deliver anti-cancer medicines. They have a spherical shape consisting of phospholipid bilayers surrounding an aqueous phase. Due to their dual nature, liposomes can use to deliver both hydrophilic and hydrophobic drugs [12]. Liposomes can efficiently deliver anti-cancer therapeutics to tumor tissues via two mechanisms: passive targeting and active targeting. Abnormal vascular nature and impaired lymphatic drainage in tumor tissues cause to passive targeting of liposomes (as nano-sized carriers) to these tissues using the effect of enhanced

CONTACT Nadereh Rahbar n_rahbar2010@ajums.ac.ir; n_rahbar2001@yahoo.com Department of Medicinal Chemistry, School of Pharmacy, Ahvaz Jundishapur University of Medical Sciences, Ahvaz, Iran; Maryam Kouchak kouchak-m@ajums.ac.ir; koochekm@yahoo.com Department of Pharmaceutics, School of Pharmacy, Ahvaz Jundishapur University of Medical Sciences, Ahvaz, Iran.

Supplemental data for this article can be accessed online at https://doi.org/10.1080/08982104.2023.2271046.

permeability and retention (EPR) [13,14]. In addition, specific ligands such as folic acid, transferrin, antibodies, growth factors, and aptamers can be conjugated onto the liposomes to achieve specific drug delivery to cancer cells [12,15]. Targeting anti-cancer drug delivery systems using ligands causes the cargo to be released intracellular by receptor-mediated endocytosis. This strategy increases therapeutic efficacy on tumor cells and may reduce the efflux of drugs out of the tumor and overcome multiple drug resistance (MDR) [16,17].

Recently, aptamers have been introduced as a new generation of targeted ligands in nanomedicine delivery systems, especially in cancer treatment [18]. Aptamers are synthetic single-stranded nucleotide sequences of RNA or DNA with a length of about 20 to 100 nucleotides and can be used instead of natural antibodies in many applications. Aptamers have a unique three-dimensional structure that is influenced by their sequence. The structure of aptamers allows target molecules to bind specifically to them with high affinity. Aptamers can be generated and selected for almost any target *in vitro* by the systematic evolution of ligands by the exponential enrichment (SELEX) method. In principle, an initial pool of oligonucleotides (10^{13}–10^{15}) is exposed to a target molecule and allowed to over-bind. Unbounded oligonucleotides are isolated and discarded, and those that bind to the target are amplified by PCR technology [19–21,22]. They have many advantages for drug targeting, including low immunogenicity, easy synthesis, and thermal stability. Due to their small size, they can easily and quickly cross through tissues and organs, allowing for rapid drug delivery [12,23,24].

Nucleolin (NCL), with an essential role in cellular activities (transcription, proliferation, and cell growth), is a non-ribosomal protein with the highest abundance in the nucleus and cytoplasm. This protein is also expressed in the cell membrane with the potential to bind to various ligands [25,26]. Overexpression of NCL in plasma membranes of large numbers of tumors and endothelial cells during angiogenesis reinforces the belief that NCL can be helpful as a tumor-specific receptor in the diagnosis and treatment of cancer [27]. In addition, the cell surface NCL acts as a protein that uptake several ligands such as growth factor, microorganism, and aptamer [26,28,29]. Surface modification of liposomes with anti-nucleolin AS1411 aptamer has been considered for tumor targeting purposes to minimize the side effects of anti-cancer drugs on healthy tissues with their particular function [30,31,32].

In situ gelling systems have attracted much attention in pharmaceutical applications. These smart polymer systems are soluble before entering the body. After administration, they undergo sol-to-gel transition under various physiological stimuli such as pH, temperature, and specific ions or molecules. Because of the unique feature of sol-to-gel transition, they can provide an injectable system with the capability to sustain and control the release of bioactive molecules. Therefore, the ease of use, sustained drug release, reduced frequency of administration, and protection of the drug against physiological conditions are among the advantages of these intelligent vehicles [33]. In contact with biological stimuli, they form a three-dimensional network consisting of chemical or physical cross-links of polymer chains that can hold significant amounts of water [34]. One of the polymers that make up *in situ* hydrogels is a poloxamer. Aqueous solutions of some poloxamers above their critical concentration possess reversible gelling properties with a uniform increase in temperature [35]. Poloxamer 407, with trademarks of Pluronic® F127 (F127) registered by BASF Laboratories, has excellent thermosensitive gelling properties [36,37].

The present study was conducted with the aim of preparing and identifying functionalized liposomes of AS1411 aptamer loaded with cobalt hydrogen arsenite ($CoHAsO_3$, CHA) in order to improve the specific efficiency of ATO on cancer cells and reduce their side effects. In addition, in order to achieve a long-term release formulation, the liposomal nanodispersion was included in the F127 solution as a thermo-sensitive *in situ* gel base. These systems were evaluated for drug release, cell uptake, cytotoxicity, histopathology, and antitumor activity.

2. Chemicals and methods

2.1. Chemicals

Cholesterol (Chol), soybean phosphatidylcholine (SPC), Calcein, poloxamer 407 (F127), dimethyl sulfoxide (DMSO), 3–(4, 5-Dimethylthiazol-2-yl)-2, 5-diphenyltetrazolium bromide (MTT), penicillin G sodium, and streptomycin sulfate were obtained from Sigma-Aldrich (Germany). AS1411 Aptamer (GGTGGGGTGGTTGTGGTGGTGGTGGTTTTTTTTTTT-Chol) was supplied by Takapouzist Company (Iran). Chloroform, methanol, ATO, and cobalt (II) acetate were from Merck (Germany). Dialysis membrane (Spectra/Por®) was provided from Biotech, USA. PBS cell culture grade was obtained from Bioidea (Iran). Dulbecco's modified eagle medium (DMEM), RPMI 1640 Medium (Roswell Park Memorial Institute), trypsin solution, and fetal bovine serum (FBS) were purchased from Gibco BRL (Gaithersburg MD, USA). Other chemicals and solvents were all of the analytical grades. Murine melanoma cell line (B16) and mouse embryonic fibroblast (MEF) were obtained from cell bank of Stem Cell Technology (Tehran, Iran).

2.2. Preparation of CHA-loaded liposomes (CHAL)

Liposomes were prepared using the thin-layer hydration method [38]. We reported the optimal synthesis method of CHA-liposomes used in this study elsewhere [24]. Briefly, SPC and Chol were dissolved in chloroform at a molar ratio of 2:1, and the solvent was removed at 45 °C using a rotary evaporator (120 rpm) under vacuum conditions to form a thin lipid layer. A mixture of Co (II) and ATO (in PBS) solutions with a molar ratio of 1:1 was vortexed for 2 min. To form a colloidal suspension of CHA (source of ATO), the mixture was kept at room temperature for two h. The obtained suspension was added to the lipid film in a rotating flask at 40 °C, and hydration was performed by slowly rotating the

flask for 30 min. The obtained liposomes were subjected to 10 cycles of freezing and thawing after sonication for 5 min. After 24 h in the refrigerator (4 °C), the unencapsulated CHA precipitate, free ATO, and Co(II) ions were separated from the liposomes by three consecutive low-speed centrifugation steps. Finally, to sediment and separate the CHA-loaded liposomes (CHAL) from the supernatant, the suspension was centrifuged at 15,000 rpm for 20 min.

2.3. Preparation of aptamer-functionalized CHA-loaded liposomes (AP-CHAL)

To fabricate aptamer-conjugated CHA-loaded liposomes (AP-CHAL), SPC and Chol were dissolved in chloroform with a molar ratio of 2:1. The solvent was evaporated entirely (45 °C) by a rotary evaporator (120 rpm) and a lipid bilayer was formed. AS1411aptamer solution (100 μM) was activated by holding at 95 °C (5 min) and then placing in an ice bath (10 min). 50 μL of this solution was mixed with the CHA suspension (Section 2.2) and incubated for 4 h at room temperature. The lipid film was hydrated with this suspension and after sonication for 5 min the formed liposomal suspension was frozen and thawed ten times. As described in the previous section, the liposomal suspension was subjected to several low-speed and high-speed centrifugation steps to remove residual CHA precipitate, free ATO, and Co(II) ions [24].

2.4. Preparation of calcein-loaded liposomes

Calcein-containing liposomes (with and without aptamer) were prepared using the lipid film hydration method, and 50 μM calcein solution was used to hydrate the solid lipid layer.

2.5. Characterization of the liposomes

2.5.1. Particle size and zeta potential measurement

Deionized water was used to dilute the liposomal samples. The dynamic light scattering (DLS) technique was used to determine the geometric mean diameter as well as the polydispersity index (PDI) of liposomes (Qodix, Scatteroscope I System, Korea). The zeta potential of liposomes was measured by a zeta sizer instrument (Malvern Instruments, UK).

2.5.2. Field emission scanning electron microscopy (FESEM)

The surface morphology of the liposomes was determined using FESEM (Mira 3 Tescan-XMU, Czech Republic).

2.5.3. Fourier transform infrared (FT-IR)

FT-IR spectra of CHAL, AP-CHAL, and ATO were recorded by a Bruker spectrometer (model Tensor 27, Germany).

2.6. Encapsulation efficiency (EE)

A furnace atomic absorption spectrometer (AA240FS/Agilent, USA) was used to determine the arsenic content of the liposomes after dilution with deionized water. A direct method was used to determine the EE of arsenic in the liposomes. The EE of arsenic in each formulation was calculated by the following equation:

$$EE\% = \left(D_l / D_i\right) \times 100 \quad (1)$$

In the above equation, D_l is the amount of arsenic loaded in the liposomes (mg), and D_i is the initial value of the arsenic atom (mg).

2.7. Preparation of F127 in situ gel systems

Various concentrations of 16, 17, 18, 20, 22, 24, 26 and 27% (*w/v*) of F127 in PBS were prepared. Afterward, the suspensions were stirred for 1 h and incubated overnight at 4 °C until the polymer was completely dissolved and a clear solution was obtained [39,40].

2.8. Determination of sol/gel transition temperature (SGT)

The physical states of different concentrations of F127 solution at the refrigerator, room, and physiological temperatures were determined after 10 min.

2.8.1. Tube inverting method

Each of the selected F127 solutions was placed in a closed 20 ml container in a water bath with constant stirring and a gradual temperature increase (0.5 degrees/min). The container was reversed horizontally every 0.5 min, and the temperature at which gelation and lack of liquid fluidity occurred through inversion of the container was recorded. This method was performed three times for each hydrogel [41].

2.8.2. Differential scanning calorimetric (DSC) method

The F127 solutions with concentrations of 18, 20, 22, and 24% (*w/v*) of F127 were prepared in distilled water at 4 °C. The blank liposomes were dispersed in F127 solutions at 4 °C, and incubated for 24 h. DSC analysis of these solutions with or without liposomes were carried out using a DSC1 STAR instrument (Mettler Toledo, Switzerland). An appropriate amount of each sample was placed in an aluminum pan (<20 mg) and heated in the temperature range of 10–60 °C at a heating rate of 5 °C/min. The DSC scans of all prepared samples were run in triplicate [40].

2.9. Preparation of in situ gels containing AP-CHAL (F127-AP-CHAL)

AP-CHAL was dispersed in F127 solution (20%) at 4 °C and incubated for 24 h [40].

2.10. In vitro evaluation of drug release

Release profiles of free ATO solution, CHAL, and F127-CHAL formulations were obtained using dialysis membrane (MW cut off 12,000 Da) method [40] in 20 ml PBS (pH 7.4) as the receptor phase at 37 °C and 70 ± 5 rpm. For this purpose, equivalent amounts of each sample (based on arsenic content) were used. 1 ml sample was withdrawn at definite intervals up to 24 h, and an equal volume of fresh release medium was replaced. The arsenic content of the samples was analyzed by atomic absorption spectrophotometry. All experiments were performed in triplicate.

2.11. Stability test

The stability of CHAL, AP-CHAL and F127-CHAL formulations was evaluated in a period of 6 months at 4 °C and at time intervals of 1, 3, and 6 months. Average particle size, PDI index and percentage of residual drug were measured.

2.12. Cell culture

B16 and MEF cell lines were grown in RPMI-1640 and DMEM cell culture media, respectively. The media were supplemented with 10% FBS and Penicillin/Streptomycin at 100 U/ml.

2.13. Evaluation of cytotoxicity

An MTT assay was used to evaluate the cytotoxicity effect of the formulations on the B16 and MEF cell lines. The cells were seeded into 96-well plates at a concentration of 5×10^3 cells/well and placed overnight at 37 °C and 5% CO_2 pressure. Then, the culture medium of each well was replaced with a culture medium containing ATO solution, CHAL, or AP-CHAL at different concentrations (0.1–10 μM based on ATO) and incubated for 24, 48, and 72 h. The cells that received the culture medium without the drug were considered as control group. At time points, the culture medium of the cells was emptied, and MTT solution (5 mg/ml) was added to each well and incubated for 4 h at 37 °C. The supernatant of the cells was removed, and the formed formazan crystals were dissolved by adding 150 μL of DMSO-producing purple dye. Finally, the absorbance of the colored solutions was measured using an Elisa reader (BioRad, USA) at 570 nm. Cell viability was calculated using Equation (2).

$$\text{Cell viability}\% = \left(\text{Abs}_{\text{sample}}/\text{Abs}_{\text{control}}\right) \times 100 \quad (2)$$

2.14. Cellular uptake of liposomal formulations

Calcein, a water-soluble dye, was used to evaluate the cellular uptake of bare and aptamer-functionalized liposomes in the murine melanoma cell line. B16 cells were seeded at a density of 1×10^6 cells/well in 6-well plates overnight. Afterward, the culture medium in each well was replaced with a culture medium containing calcein, calcein-loaded liposomes, and calcein-loaded aptamer-functionalized liposomes and incubated at 37 °C for 1 and 3 h [42]. At predetermined time points, the cells were washed several times with PBS (pH 7.4). The photographs of the cell plates were obtained using a fluorescent microscope (IX71-OLYMPUS, Japan).

2.15. In vitro experiments

In this study, male BALB/c mice (6–8 week-old) with a weight range of 28–35 g were used. They were obtained from the animal center of Ahvaz Jundishapur University of Medical Sciences (AJUMS), Iran. Mice were kept on a 12-h-light/12-h-dark cycle with the room temperature maintained at 25 °C. The guideline of Ethics Committee of AJUMS (IR.AJUMS.REC.1399.042) was used for all animal experiments.

2.15.1. Creating of tumor model

B16 cell suspension at the density of 4×10^6 cells/ml was prepared in the culture medium, and each mouse was inoculated with less than 100 μL of this suspension subcutaneously on the dorsal sides of the mice. After the tumors had reached about 400 mm^3, the mice were randomly divided into saline, ATO, CHAL, AP-CHAL, and F127-AP-CHAL groups for treatment.

2.15.2. In vitro antitumor activity

Tumor-bearing BALB/c mice were treated when tumors grew to ≥100 mm^3 (on the 8th or 10th day). Mice were randomly divided into nine groups with six mice in each group. From the first to the ninth group, mice received normal saline, ATO solution (6 and 8 mg/kg), CHAL (8, 10, and 16 mg/kg), AP-CHAL (10 mg/kg), and F127 *in situ* gel (10 mg/kg), respectively. Tumor-bearing BALB/c mice received seven injections subcutaneously peri-tumorous (into normal tissue surrounding the tumor with a distance of about 2 mm from the tumor periphery (twice a week for 21 days. The weight of the mice was recorded before receiving each dose. Also, the dimensions of tumors were measured with a caliper, and then tumor volume was calculated using the Equation (3).

$$V = x \times y^2/2 \quad (3)$$

In this equation x and y represents the large and small diameter of the tumor, respectively. Following the death of each mouse, tumor tissue and the main organs were isolated. After weighing the cancerous mass, the organs and tumor were sliced and stained with hematoxylin and eosin (H&E) for histopathological evaluation.

Mice that survived until the end of the treatment period (21 days) were euthanized by ketamine (45 mg/kg) and xylazine (9 mg/kg) after nine days. Tumors were weighed and collected with other major organs for sectioning and stained with H&E.

The inhibition rate (IR) of tumor growth for each formulation was calculated based on Equation (4).

$$\text{IR} = (1 - W_t/W_c) \times 100 \quad (4)$$

In this formula, W_t and W_c refer to the average tumor weight of the treated group and the control group, respectively.

2.16. Statistical analysis

All the experiments were performed in triplicate, and data were expressed as mean ± standard deviation (SD). The analysis of variance (ANOVA) test was used to compare the results and evaluate the statistical significance. p Values less than 0.05 ($p < 0.05$) was considered as a criterion of statistical significance [38].

3. Results and discussion

3.1. Characterization of the liposomal systems

The FESEM images (Figure 1(AI,AII)) show that the formed CHAL and AP-CHAL are spherical and have dimensions of less than 200 nm, which is a proper size for drug targeting [17]. As shown in Figure 1(B), the EDX spectrum of CHAL confirms the presence of P, N, O, C, and As in the liposomal structure. Furthermore, the strong the arsenic peak proves that arsenic is trapped in CHAL with high efficiency. According to DLS results, the average particle size of liposomes without and with aptamer was about 76 and 116 nm, respectively. The larger size of the latter could be due to the conjugation of aptamer with liposomes, which leads to an increase in their hydrodynamic diameter [43]. In addition, both liposomal samples showed PDI values <0.5. The zeta potential values of CHAL and AP-CHAL show a higher negative charge for AP-CHAL, which were −0.64 mV and −2.95 mV, respectively. The negatively charged groups in the AS1411 aptamer structure could be responsible for this zeta potential difference between the liposomal formulations [44]. Akhtar et al. reported similar results by introducing an optimized ATO liposomal formulation with a size of about 100 nm and partial negative charge [45]. The mean particle sizes, PDIs, and zeta potentials of CHAL and AP-CHAL are presented in Table 1. FT-IR spectra of ATO (Figure 1(CI)), CHAL (Figure 1(CII)), and AP-CHAL (Figure 1(CIII)) are presented in Figure 1(C). As seen in Figure 1(CI), a relatively sharp and strong peak at 657 cm^{-1} wavenumber can be attributed to the absorption peak of arsenic. Besides, the absorption peak of the stretching vibration of the O–H bond

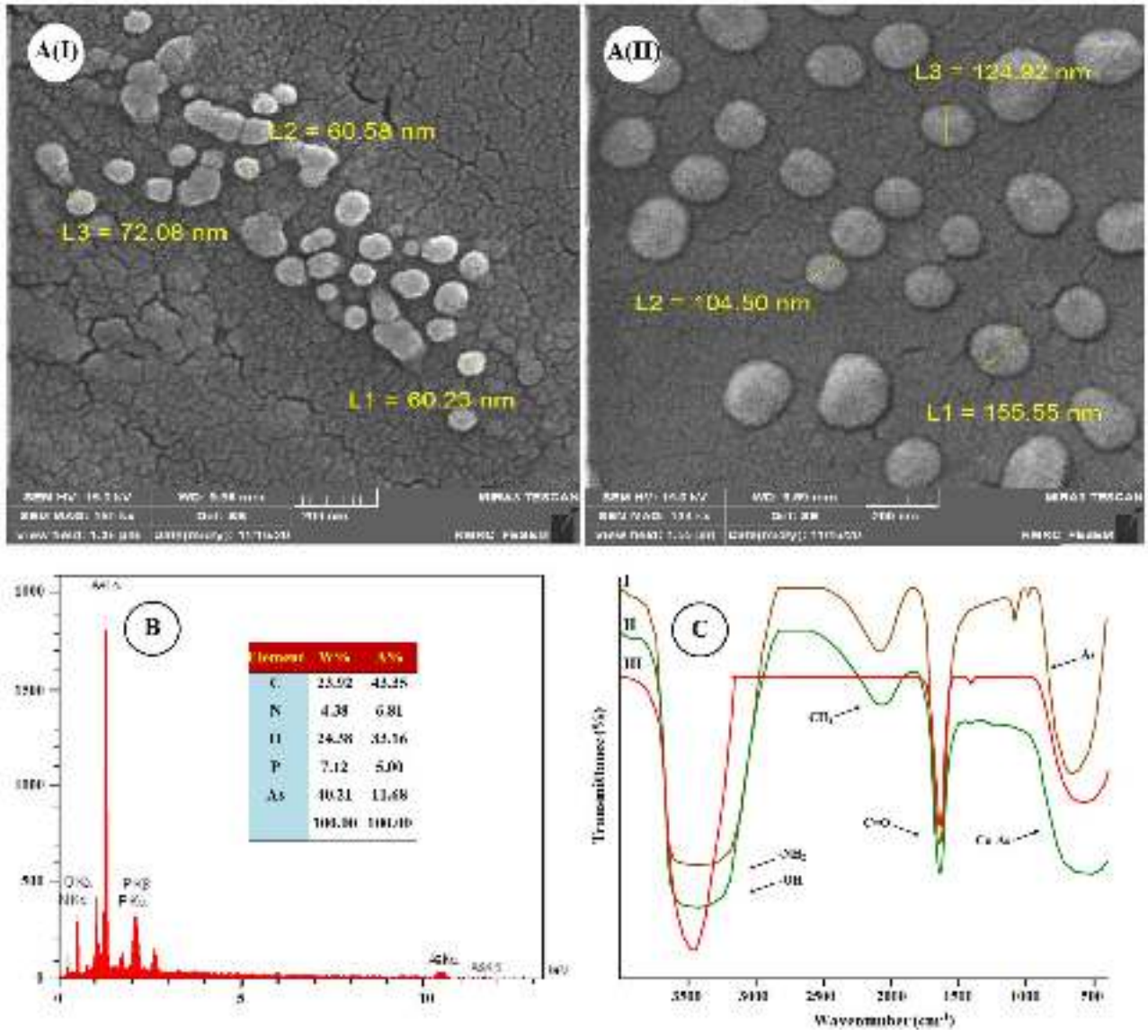

Figure 1. FESEM images of CHAL (AI) and AP-CHAL (AII); EDX spectrum of CHAL (B); FT-IR spectra of ATO (CI), CHAL liposomes (CII), and AP- CHAL (CIII).

in ATO can be at 3432 cm^{-1} [46]. The peaks related to arsenic in CHAL and AP–CHAL spectra are shifted to 570 and 578 cm^{-1}, respectively (Figure 1(CII,CIII)). The formation of arsenic-cobalt bond in liposomal formulations can be a reason for this observation. In addition, the peaks at 3435 and 3468 cm^{-1} in these spectra could be due to the stretching vibrations of the O–H, N–H, and C–H bonds in the Chol and SPC content of the liposomal formulations. The absorption zone at the 2068 cm^{-1} peak can relate to CH_2 vibration. Further, the sharp absorption peak at 1635 cm^{-1} is characteristic of the stretching vibration of C=O bond [47,48].

3.2. Encapsulation efficiency of the liposomal formulations

The EE of CHAL and AP-CHAL are 60.2 ± 6.5% and 58.7 ± 4.2%, respectively, and there was no significant difference between them ($p = 0.252$). The rapid release of drugs with low molecular weight is a drawback of many liposomal formulations. In aqueous solutions, ATO exists as $As(OH)_3$ (H_3AsO_3) chemical form; therefore, ATO-loaded liposomes are unstable due to the fast diffusion of $As(OH)_3$ through the liposomal lipid bilayer, which reduces drug loading efficiency in the stage of lipid layer hydration [49]. Different strategies were introduced to solve this problem. In our previous study [24], ATO was loaded into liposomes using three methods, including active loading, passive loading, and passive loading of CHA (As source). The latter method showed the highest loading efficiency. In this strategy, Co (II) and hydrogen arsenite ($HAsO_3^{2-}$) form a low-solubility precipitate before exposure to the lipid-thin film. During the self-assembly of the nanocarriers in the presence of the colloidal CHA suspension, $CoHAsO_3$ is trapped in the liposomes. Due to the low solubility of the $CoHAsO_3$ precipitate, As cannot diffuse quickly, which leads to a significant increase in loading efficiency.

Table 1. Particle size, PDI, and zeta potential of the liposomal formulations.

Formulation	Particle size (nm)	PDI	Zeta potential (mV)
CHAL	76.7	0.49	−0.64
AP-CHAL	116	0.45	−2.95

3.3. Sol/gel transition temperature of F127 solutions

All F127 solutions were in the liquid state at low temperatures, but at higher temperatures, they showed a concentration-dependent sol/gel transition (Table S1). The SGT of F127 solutions was determined by the tube inverting method. F127 solutions, including 18, 20, 22, and 24% (*w/v*), were converted from liquid phase to gel phase in 1–2 min at 29, 27, 25, and 23 °C, respectively. There was an inverse relationship between the SGT and the F127 concentration, which is consistent with the other reports [50,51]. Due to the lack of gel formation at room temperature and the rapid conversion of sol to gel within a few seconds, a concentration of 20% poloxamer F127 was selected as the appropriate concentration.

3.4. Determination of thermo-gelation properties of F127 solutions using DSC

The DSC thermograms of the selected F127 solutions (18, 20, 22, and 24%, *w/v*) with and without liposomes were obtained to analyze the thermogelation properties of F127 solutions, and also investigate the interaction between liposomes and F127 (Figure 2). All F127 samples present a definite endothermic peak indicating the critical micelle temperature (CMT). Figure 2(A) shows that as the concentration of F127 increases, phase transition temperature lowers. With increasing temperature, the copolymer chains begin to form micellar structures due to dehydration of the hydrophobic propylene oxide (PPO) blocks of F127, known as the initial stage of gel formation [52,53]. In other words, these systems are liquid at low temperatures and start to harden as a gel at high temperatures. Figure 2(A) also shows a smaller peak at a higher temperature for each thermogram, representing SGT. These results are consistent with previous findings [52,54,55]. As seen in Figure 2(A), both CMT and SGT peaks are shifted to higher temperatures in samples containing liposomes. This finding indicates that the phase behavior of this system is affected by liposomes.

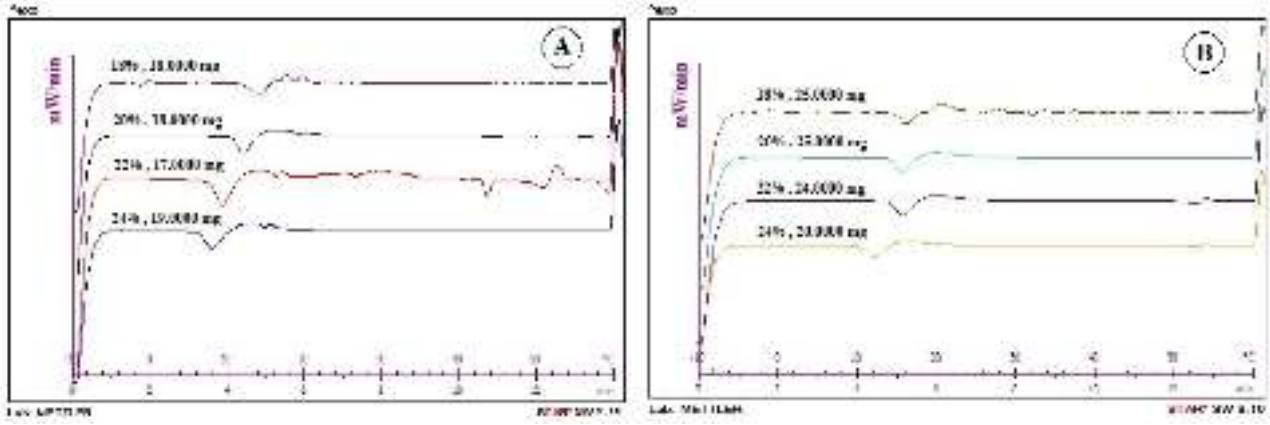

Figure 2. DSC thermograms of different concentrations of pure F127 solutions (A) and F127 solutions containing liposomes (B) at the heating rate of 5 °C/min.

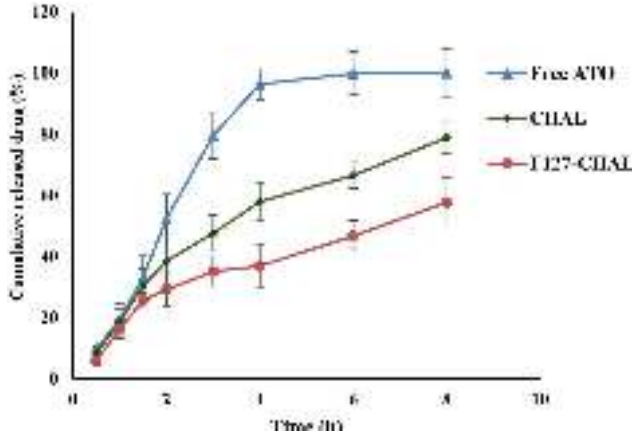

Figure 3. *In vitro* drug release profile of free ATO, CHAL, and F127-CHAL at pH 7.4 ($n = 3$).

3.5. In vitro *drug release*

As shown in Figure 3, ATO is completely released from the free ATO solution through the dialysis membrane within 4 h, while the drug release rates from both CHAL and F127-CHAL are lower, and after 8 h do not reach 100%. There are significant differences between the 8-h drug released from three formulations ($p < 0.05$). The slow drug release from CHAL is due to the presence of the drug in the form of $CoHAsO_3$ precipitate in the liposome vesicles, which has limited solubility and low dissolution rate. Of course, the high encapsulation efficiency of this formulation can be due to the presence of this low-soluble precipitate in the liposomes, which, in addition to maintaining the stability of the drug, enables the slow and continuous release of the drug. This property can increase the residence time of the drug at the tumor site. The drug release process from F127-CHAL is much slower than that of CHAL, which showed 95.4% within 24 h. In this formulation, in addition to the slow rate of dissolution and release of CHA from the liposome, F127, which turns into a gel at 37 °C, acts as a diffusion barrier and provides a sustained release profile up to 68% in 24 h.

3.6. *Stability test results*

The results of the stability investigation indicate the physical and chemical stability of the formulations during 6 months (Tables S2 and S3). The particle size of the formulations increased slowly during 6 months, which could be related to their low zeta potential. This increase was less in the case of AP-CHAL, which had a higher zeta potential value. AP-CHAL showed a 20% increase in particle size within 6 months, with an average particle size of about 139 nm suitable for targeted drug delivery.

3.7. *Evaluation of cytotoxicity:* in vitro *studies*

B16 cells were incubated in the presence of ATO solution at different concentrations and harvested at different exposure times (24, 48, and 72 h) for analysis using the MTT method. Figure 4 shows that ATO inhibits the viability of B16 cells in a time and concentration-dependent manner. At the

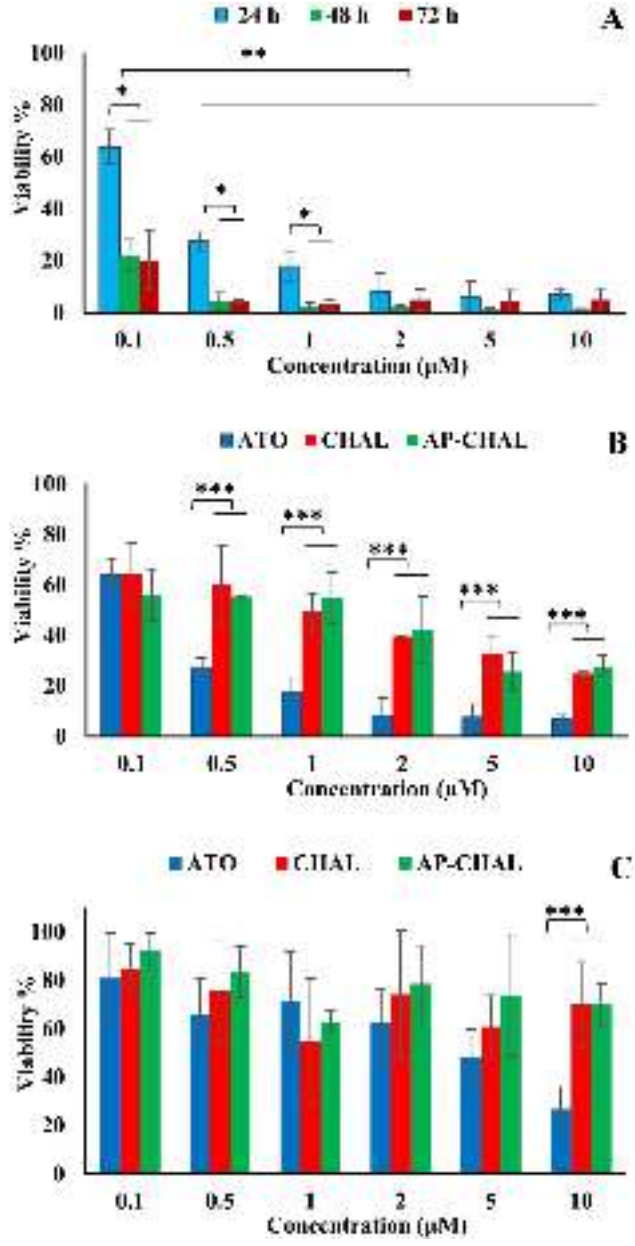

Figure 4. The viability of B16 cells at different times of exposure to free ATO (A), and cytotoxicity effect of free ATO, CHAL and AP-CHAL on B16 cells (B) and MEF cells in 24 h (C). (*significant difference in cell viability after 24 h compared to 48 and 72 h ($p < 0.001$). **significant difference in cell viability at 0.1 μM ATO concentration compared to other doses. ***significant difference in cell viability of free ATO compared to CHAL and AP-CHAL).

minimum concentration of ATO (0.1 μM), cell viabilities were 63.80, 22.07, and 20.23%, respectively, after 24, 48, and 72 h of exposure, but at higher concentrations, the viability reduced significantly. This phenomenon was also reported by Liu et al. They observed the apoptosis and inhibition of proliferation of H22 hepatocellular carcinoma and bovine aortic endothelial cells (BAEC) by ATO in a time- and dose-dependent behavior [56].

Various cell pathways are affected by different levels of ATO, including proliferation, differentiation, cell death via apoptosis or necrosis, inhibition or acceleration of angiogenesis, and reactive oxygen species [6,56,57]. At low concentrations, it induces altered gene expression and increases cell

proliferation, while high concentrations of ATO and its metabolites can cause genomic damage by inhibiting DNA repair [58,59,60]. ATO has been found to induce relative differentiation at concentrations of 0.1–0.5 μM, while at 0.5–5 μM, cell death occurs through the apoptosis mechanism. However, treatment with ATO at levels higher than 5 μM may cause cell death via acute necrosis [60–62]. According to the other reports, at low doses (≤1μM), an ATO-induced differentiation occurred in retinoblastoma and neuroblastoma cells via ERK1/2 activation, whereas ROS-induced apoptosis was the reason for cell death in both cell lines at high doses (≥2 μM) [63]. Therefore, ATO has multiple mechanisms to affect cells. Our results showed that at low concentrations of ATO (0.1 μM), the survival level is significantly higher than at higher concentrations due to two simultaneous processes of proliferation and cell death (apoptosis). Differentiation of cancer cells into normal cells could be another reason for high cell viability at low ATO concentrations [10]. As seen in Figure 4(A), the lethal effect of ATO is more pronounced after 48 and 72 h incubation due to the increased exposure time.

In the next step, the cytotoxicity effect of ATO solution, CHAL, and AP-CHAL at different concentrations on two cell lines, B16 and MEF, was compared (Figures 4(B,C)). As shown in Figure 4(C), ATO at different concentrations showed different behavior against MEF cells. There was no significant difference in viability between applied concentrations up to 2 μM. However, at higher concentrations (5 and 10 μM), MEF viability decreased significantly ($p < 0.05$) might be due to the necrosis caused the cell death at these concentrations. In addition, ATO appears to have cell-dependent cytotoxicity effects. At the same concentrations, ATO solution shows a lower inhibitory effect on MEF cells than the B16 tumor cell line. MEF cells exposed to all three formulations showed significantly greater viability than B16 melanoma, indicating their genetic differences in response to external stimuli in generating signals to activate or suppress critical cellular pathways. Similarly, Liu et al. observed different levels of effect on H22 and BAEC cells so that at similar concentrations of ATO, H22 tumor cells were more susceptible to apoptosis than the latter [56]. In another study, ATO was found to inhibit the proliferation of human uveal melanoma cells more potently than normal human fibroblast cells in a dose- and time-dependent manner. They showed that ATO-induced apoptosis in the uveal melanoma cell line was mainly mediated through mitochondria in the dose range used (5–50 μM) [63]. Various levels of ATO-induced apoptosis were shown in cells with different intracellular glutathione (GSH) levels. Cells with the lowest glutathione content are more sensitive to arsenite. ATO-induced cell death, which is mediated by ROS, can be further attenuated by glutathione [64].

Treatment with CHAL and AP-CHAL significantly increased the viability of B16 cells compared to the cells treated with free ATO (Figure 4(B)). However, there was no significant difference in the viability of the cells treated with both liposomal formulations. This finding is consistent with our previous research in which no significant difference was observed in the viability of HT-29 cancer cells treated with CHA-containing liposomes with or without AS1411 aptamer [24]. The same mechanism of action for cell death and slow drug release of both liposomal formulations may be the reasons for this phenomenon. The low solubility of CHA and its slow release from the liposomes creates a low concentration of the drug in the cellular environment, which makes the conditions suitable for cell differentiation and proliferation. Similar results were seen for fibroblast cells (Figure 4(C)).

3.8. Cellular uptake of liposomes

The EE of calcein-loaded liposomes and calcein-loaded aptamer-functionalized liposomes were 62.7 ± 4.5% and 64.5 ± 2.7%, respectively, and there was no significant difference between them ($p > 0.05$). Calcein a water-soluble dye was used to evaluate the cellular uptake of liposomes with and without aptamer in B16 cells. As shown in Figure 5(A), free calcein can enter the cells. The low molecular weight (MW = 622.5 g/mol) of the calcein molecule facilitates its penetration into the cells through a diffusion mechanism.

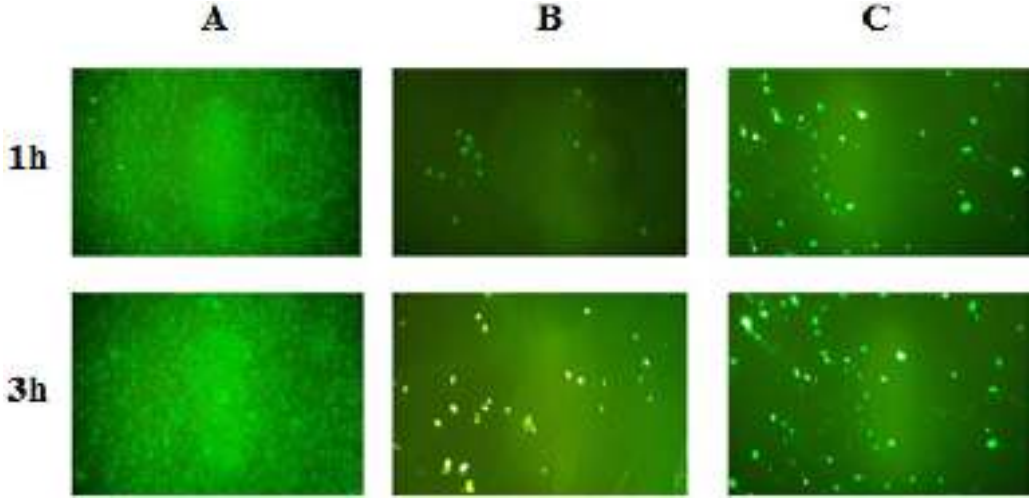

Figure 5. The fluorescence microscopy images of B16 cells after 1 and 3 h of treatment with calcein solution (A), calcein-loaded liposomes (B), and calcein-loaded aptamer-functionalized liposomes (C) at 37 °C (microscopic images are shown at 100× magnification).

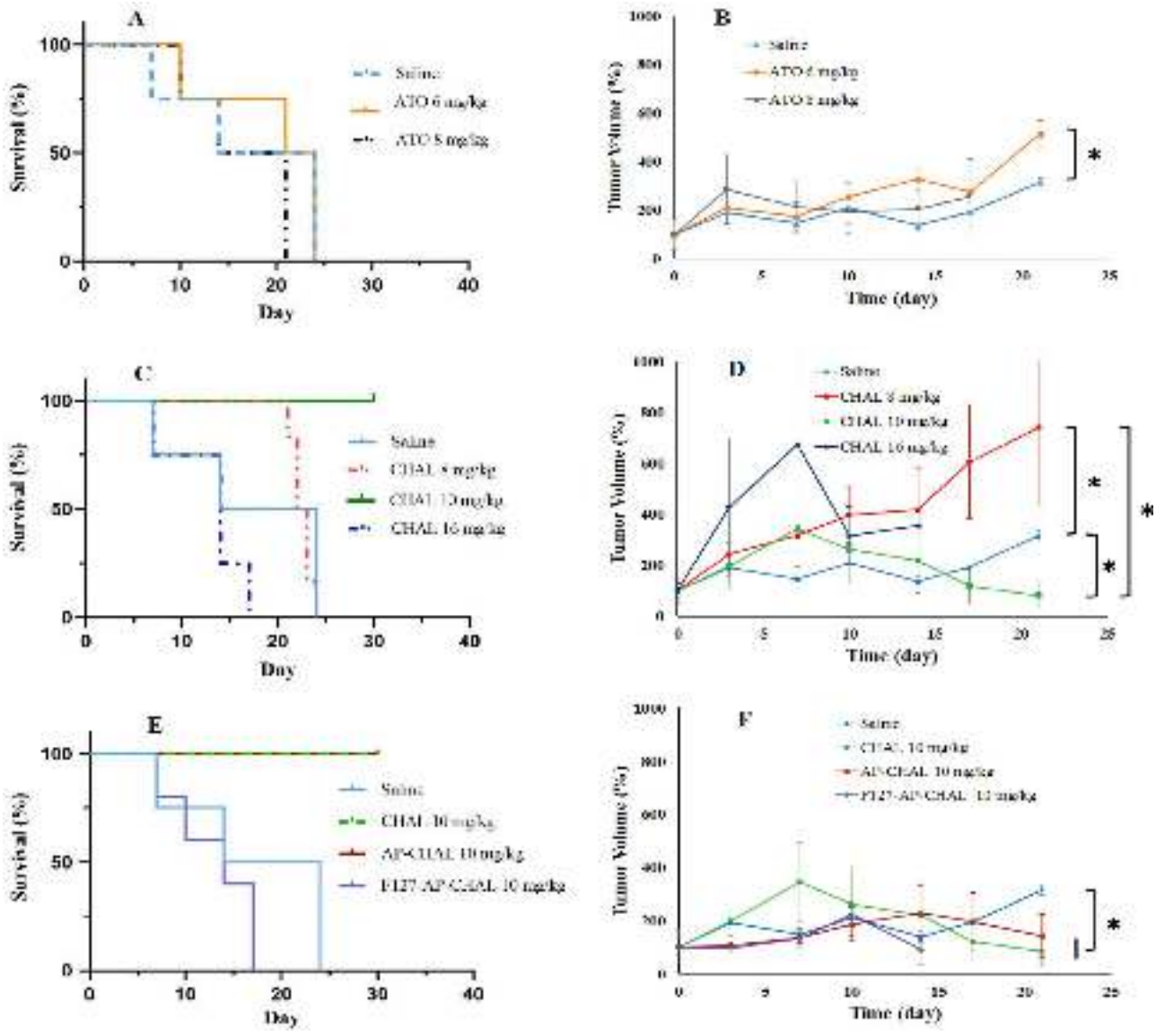

Figure 6. Survival curve and tumor volume after subcutaneous injection of ATO 6 and 8 mg/kg (A and B); CHAL 8, 10, and 16 mg/kg (C and D); CHAL 10 mg/kg, AP-CHAL 10 mg/kg, and F127-AP- CHAL (E and F). Saline group was considered as control. (*statistically significant different: $p < 0.05$).

Microscopic images of calcein-containing liposomes (Figure 5(B,C)) show large bright spots, indicating cellular uptake of intact liposomes. From the obtained results, it can be concluded that the entry of liposomes into the cells was through endocytosis. This pathway is time-dependent such that cellular uptake of calcein is more significant after 3 h compared to after 1 h. The abundance and dot density of aptamer-conjugated liposomes are more significant than non-conjugated liposomes. These results confirm the effectiveness of aptamer-functionalized liposomes in enhancing cellular uptake, which can be used for the targeted release of chemotherapeutic agents in tumor-specific cancer treatment. Reyes-Reyes et al. proved that the uptake of anti-NCL AS1411 occurs through macropinocytosis in cancer cells [65]. NCL plays an essential role in inducing macropinocytosis in cancer cells due to its overexpression in the plasma membrane of many cancerous cells [25]. Therefore, the considerable difference in cell uptake of liposomal formulations can be evidence of the entry of aptamer-functionalized liposomes through the NCL-induced macropinocytosis pathway, which is more efficient than simple endocytosis [65].

Although the cell uptake results in Figure 5 confirm the effectiveness of liposomes functionalized with aptamer in increasing cell uptake, in Figure 4(B), no significant difference in the viability of cells treated with CHAL and AP-CHAL is observed. The difference in these data is related to the difference in the time periods of the experiments. Cell uptake tests was performed in 3 h and MTT experiments in 24 h. In the first hours when cells are exposed to the formulation, the presence of nucleolin aptamer in AP-CHAL causes more cellular uptake of liposomes. However, 24 h can be enough time to compensate for the initial slowness of entry the CHAL formulation through the entry routes of nonfunctional liposomes into the cell, and finally, the same viability of the two formulations was observed in 24 h. However, the real

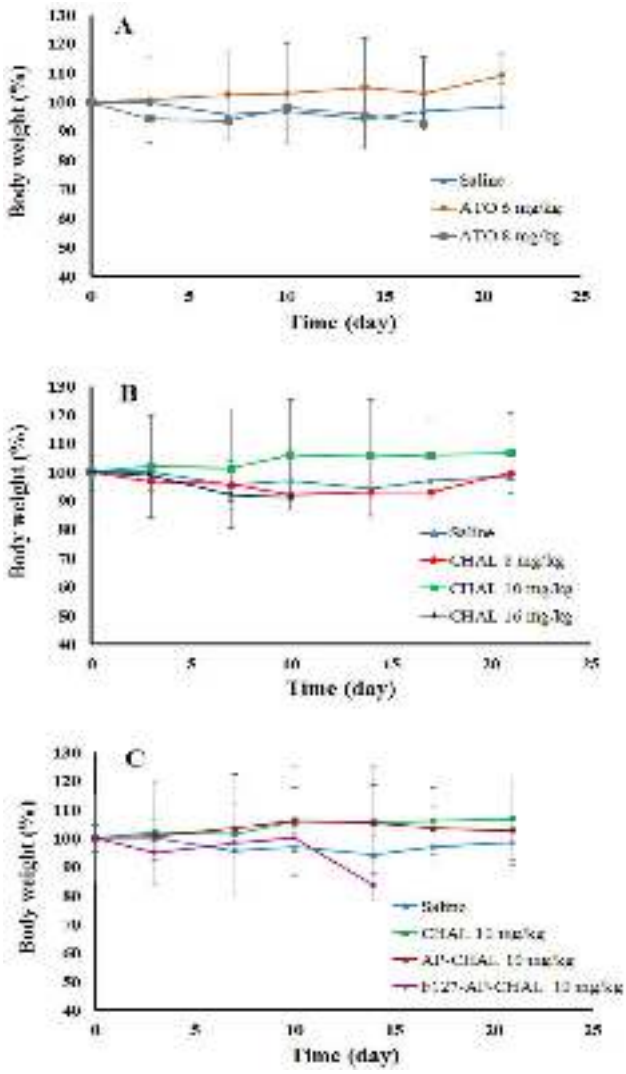

Figure 7. Body weight changes during 21-day treatment with free ATO (A), CHAL (B), AP-CHAL, and F127-AP-CHAL (C).

difference between the two formulations can be seen in long-term *in vivo* tests.

3.9. In vivo *antitumor activity of different formulations*

The antitumor efficacy of free ATO, CHAL, AP-CHAL, and F127-AP-CHAL was evaluated in B16 tumor-bearing BALB/c mice by determining changes in tumor volume, survival of the animals, and histopathology data. In addition, body weight changes during the treatment period were measured to assess the toxicity of the formulations. In each test group, tumor sizes and body weights were normalized to their initial values [66]. The tumor volume of the negative control (saline) group that was untreated mice and received sterile isotonic normal saline had an increased trend. The mice died over time, and at the end of the 21 days, only 50% survived (Figure 6).

Mice receiving doses of 6 and 8 mg/kg free ATO died gradually during the treatment. At the end of the 21st day, 50% of the 6 mg/kg group survived, while no mice survived in the 8 mg/kg group (Figure 6(A)). The tumor volume in group 6 mg/kg showed more growth than in the control group and group 8 mg/kg (Figure 6(B)). Increasing evidence has supported the promotion of tumor growth by low doses of ATO. When ATO is administrated at low doses, it may stimulate tumor angiogenesis and vascular endothelial growth factor (VEGF) expression in H22 tumor tissue and B16 melanoma, as well as up-regulate differentiation of retinoblastoma and neuroblastoma cells [56,63].

It seems that subcutaneous injection twice a week of a 6 mg/kg dose creates a low systemic concentration of ATO, which activates the angiogenesis and proliferation processes in tumor tissue. Considering that subcutaneous injection needs to release the product in the extracellular matrix to reach the blood, it delays the delivery to the target tissue. It thus shows a lower systemic efficiency than intravenous injection (Figure 6(B)). However, the higher dose in group 8 mg/kg gradually increases ATO plasma level and activates the mechanisms of cell death. Besides being toxic to tumor cells and reducing their growth, ATO probably damages the vital tissues of the mice and results in body weight loss (Figure 7(A)) and early death (Figure 6(A)).

Mice receiving CHAL 8 mg/kg showed considerable tumor growth and survival, so that only one mouse died until 21st day (Figure 6(C,D)). It can be attributed to the slow and time-dependent uptake of liposomes by tumor cells through the endocytosis mechanism and the low solubility of CHA, which creates a low concentration of ATO in the tumor environment resulting in ATO-induced proliferation.

All mice in the CHAL 10 mg/kg group survived to the end of treatment (Figure 6(C)) and showed body weight gain (Figure 7(B)). Although the tumors increased in size up to the 7th day, they began to shrink after that, so that the tumor protrusion was not palpable from the 17th day in one mouse, and on the last day in three mice (Figure 6(D)). In the early days, subcutaneous injection of CHAL and slow endocytosis of liposomes deliver a low concentration of drug to the malignant cells, which activates angiogenesis and proliferative mechanisms. As a result of continued drug administration, the liposomes tend to accumulate in tumor vascular areas due to the EPR effect, and anti-angiogenesis and apoptosis pathways are activated, leading to the death of tumor cells. Compared with free ATO, CHAL 10 mg/kg showed a more remarkable survival and inhibitory effect on B16 tumor tissue owing to a) the tight encapsulation of ATO in the form of CHA in liposomes which provides a long circulation period, and b) the EPR effect that enables passive targeting of solid tumors by nanoparticles. CHAL 16 mg/kg caused high mortality in mice, and all of them died before the 17th day (Figure 6(C)) because the dose exceeded the toxic limit.

A distinct antitumor effect was observed in the AP-CHAL-treated group. As seen in Figure 6(E), all mice receiving AP-CHAL 10 mg/kg survived even to the end of the treatment period. Unlike the other treatments, the tumor volume of the AP-CHAL group did not significantly change during the treatment and gradually shrunk after 14 days, so that the tumor protrusion completely disappeared in 50% of the mice (Figure 6(F)). In addition, the body weight of the mice increased slightly, which indicated the general health of the

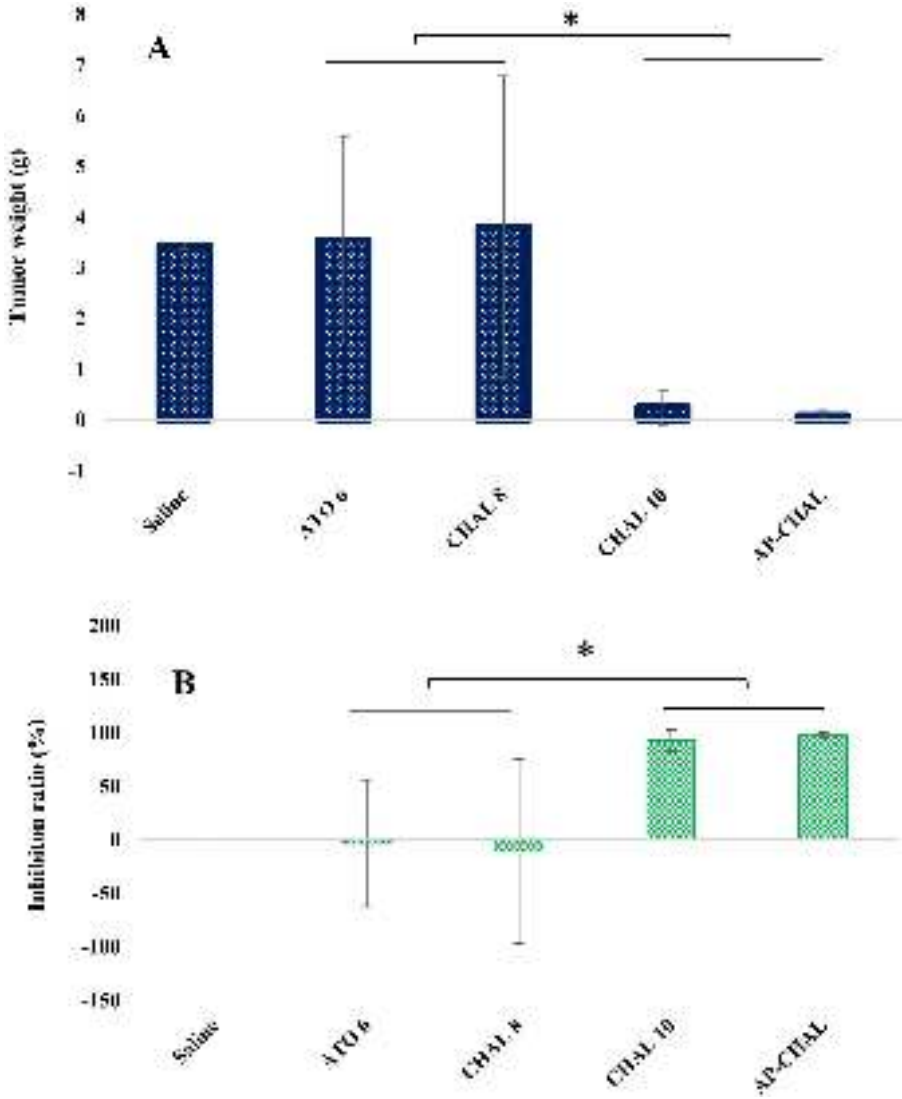

Figure 8. Tumor weight (A) and inhibition rate (IR) of tumor growth (B) in control, ATO, CHAL, and AP-CHAL groups. (*statistically significant different: $p < 0.05$).

mice in group AP-CHAL (Figure 7(C)). In the AP-CHAL and CHAL groups with 10 mg/kg dose, the animals were still alive after 30 days (Figure 6(E)). However, AP-CHAL, unlike CHAL, did not increase tumor volume at the beginning of the treatment. Macropinocytosis appears to be caused by the activation of the NCL-aptamer link, which accelerates the cellular uptake of AP-CHAL and creates a high concentration of ATO inside the tumor cells resulting in the cell death process from the start of the treatment.

F127-AP-CHAL presented disappointing results. For unknown reasons, the mice showed significant weight loss after treatment (Figure 7(C)). The tumor size in these animals had a growing trend, and the mice began to die on the 7th day, with none surviving to the 17th day (Figures 6(C,E). The images of mice treated with normal saline, ATO 6 mg/kg, CHAL 8 mg/kg, CHAL 10 mg/kg, and AP-CHAL 10 mg/kg in the beginning, duration, and end of the treatment period are presented in Fig. S1.

Figure 8 shows the weight of isolated tumor tissues (Figure 8(A)) and the inhibition rates (IR) (Figure 8(B)) of different treatments. The IR of ATO 6 mg/kg, CHAL 8 mg/kg, CHAL 10 mg/kg and AP-CHAL 10 mg/kg are −3.2, −10.47, 92.73 and 97.67%, respectively. ATO 6 mg/kg and CHAL 8 mg/kg treated groups show negative IR values revealing tumor volume increases compared to the control group at the end of treatment. The high IR value for AP-CHAL may be due to the binding of the AS1411 aptamer ligand to the NCL receptor. The tumor tissues isolated from mice are shown in Figure S2.

3.10. Histopathology study

In the saline group, a large number of polygonal proliferated cells with different sizes were observed. The individual cells had an abundant cytoplasm with distinct cell margins and variable amounts of intracytoplasmic melanin. Nuclei were often vesicular and in the center. The high ratio of nucleus to cytoplasm in these cells indicates pleomorphism in such a way that the nuclei had different shapes and very different sizes with many nucleoli. Also, many mitotic figures were

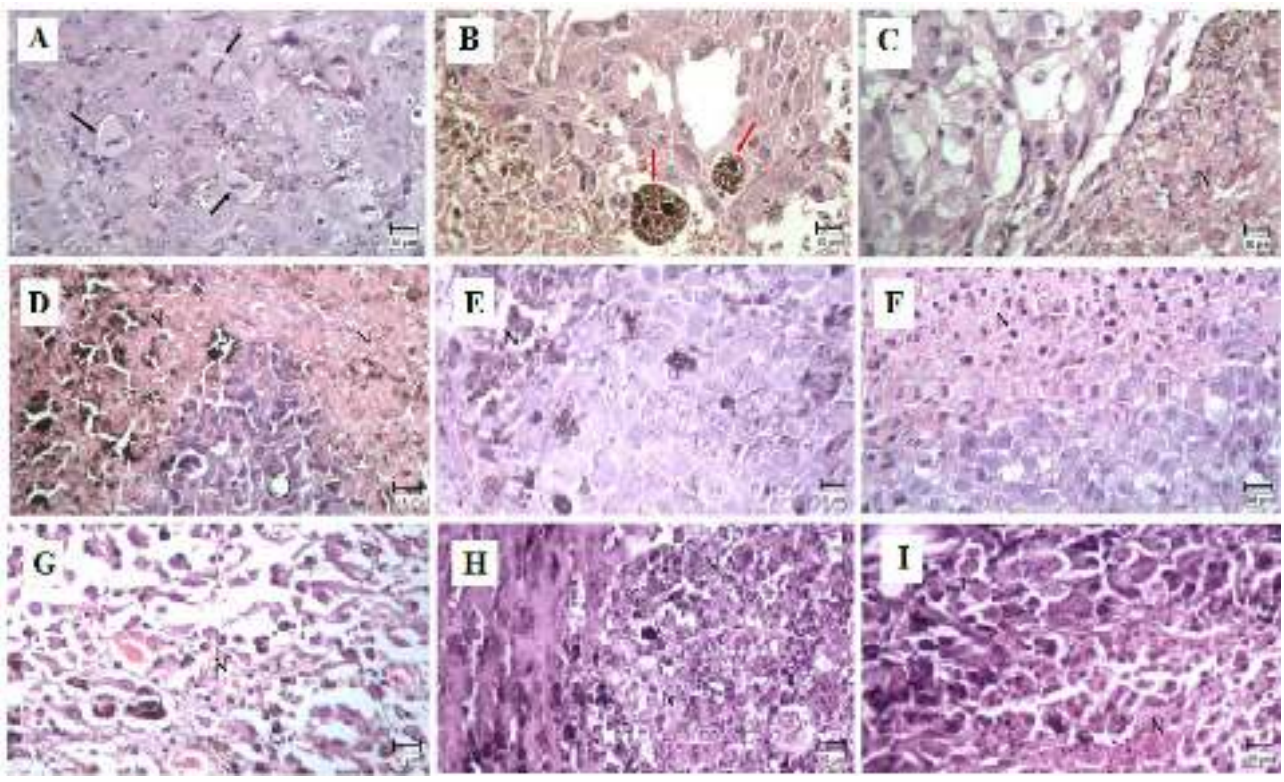

Figure 9. Photomicrographs of the tumor in different groups: saline (A and B), ATO 6 mg/kg (C), ATO 8 mg/kg (D), CHAL 8 mg/kg (E), CHAL 10 mg/kg (F), CHAL 16 mg/kg (G), AP-CHAL 10 mg/kg (H), and F127-Ap-CHAL (I). (Note: Mitotic figures (black arrows); large cells containing melanin (red arrows); necrosis area (N); hematoxylin and eosin staining).

seen among the cells (Figure 9(A)). Small foci of necrosis were visible among the tumor cells. Large cells containing melanin were also observed among the foci of necrosis (Figure 9(B)).

As seen in Figure 9(C), extensive necrosis of tumor cells is observed in ATO 6 mg/kg group, and a large part of the necrosis was located in the center of the tumor mass. Tumor cells around the necrosis area also showed severe cell swelling and fat change. In addition, a small number of tumor cells is visible around the necrosis area. In the ATO 8 mg/kg group, necrotic areas were more extended (Figure 9(D)). In the CHAL 8 mg/kg group (Figure 9(E)) an area of necrosis was seen. These foci showed coagulation necrosis of tumor cells. These cells had pycnotic nuclei with a more colorful cytoplasm than normal cells. The integrity of the tumor cells was lost, and the empty spaces between them were visible (the tumor cells disintegrated). As can be seen in Figure 9(F), in CHAL 10 mg/kg group, the highest rate of necrosis of tumor cells was observed, and a limited number of tumor cells were observed around the necrosis area. In CHAL 16 mg/kg group, all tumor cells were necrotic (Figure 9(G)). In Ap-CHAL 10 mg/kg group, the minimum rate of tumor cells was seen, and most of them were destroyed (Figure 9(H)). In the F127-AP-CHAL group, necrosis was seen, but it was less than the AP-CHAL group (Figure 9(I)).

Sections prepared from different tissues were subjected to microscopic examination to evaluate the toxicity of different formulations. ATO 8 mg/kg group (Figure S3A) and CHAL 16 mg/kg group (not shown) led to extensive necrosis in kidney tissues. Also, extensive necrosis of liver hepatocytes was seen in the liver after treatment by ATO 8 mg/kg (Figure S3B). No significant microscopic changes were observed in other groups compared to the control group.

4. Conclusions

ATO (Trisenox) is an approved first-line treatment for APL. However, ATO has been shown to have poor performance in treating solid tumors, such as dose-limiting toxicity, rapid renal clearance, and high serum protein binding. To address this concern, two liposomal formulations, CHAL and AP-CHAL, have been developed to deliver ATO to solid tumors. Very favorable results of CHAL 10 mg/kg and AP-CHAL 10 mg/kg anti-cancer drug delivery systems were high tumor growth inhibition and tumor disappearance in many mice without any noticeable side effects, weight loss, or death during treatment. In addition, there were no noticeable pathological changes in different organs. Although these two formulations, compared to free ATO, successfully restrained melanoma cancer in treated mice, they showed less growth inhibition in the B16 cell culture. The inconsistency of cell culture data and *in vivo* results can be attributed to the difference in the pharmacokinetics of free and liposomal ATO. Free ATO molecules, due to their small size, have a fast renal elimination and their concentration in blood circulation decreases quickly. Therefore, higher doses are needed to reach the therapeutic concentration of drug in the tumor tissue, which leads to the toxicity of healthy organs. In contrast,

liposomal forms facilitate selective tumor accumulation via the EPR effect. On the other hand, the anti-angiogenesis effect of the drug, which is one of the mechanisms of inhibiting tumor growth, occurs *in vivo*. Both liposomal formulations have two desirable properties of a drug delivery system, including targeted delivery and controlled release, which play a vital role in the delivery of anti-cancer drugs. The increase in tumor size in CHAL-treated mice at the beginning of the treatment, unlike AP-CHAL, suggests an accelerated cellular uptake of the latter formulation, resulting in a high internal ATO concentration in tumor cells. The superiority of the aptamer-functionalized formulation could be related to the activation of NCL-aptamer binding in cancer cells, inducing macropinocytosis, which bypasses the MDR process as well as enhancing cellular uptake. Therefore, due to its high efficiency in inhibiting the growth of solid tumors and minimal toxic effects on healthy tissues, AP-CHAL can be used as an effective drug delivery system with considerable potential in treating solid tumors.

Acknowledgements

The authors wish to thank for financial support of this research work by Research Council of Ahvaz Jundishapur University of Medical Sciences Nanotechnology Research Center. This article is extracted from the thesis of Dr. Fatemeh Shariat Razavi.

Ethical approval

Ahvaz Jundishapur University of Medical Sciences Ethics Committee guidelines with reference number IR.AJUMS.REC.1399.042 were used for all animal experiments.

Disclosure statement

No potential conflict of interest was reported by the author(s).

Funding

The authors wish to thank for financial support of this research work by Research Council of Ahvaz Jundishapur University of Medical Sciences Nanotechnology Research Center with [grant number N-9908].

References

1. Dilda PJ, Hogg PJ. Arsenical-based cancer drugs. Cancer Treat Rev. 2007;33(6):542–564. doi: 10.1016/j.ctrv.2007.05.001.
2. Jolliffe DM. A history of the use of arsenicals in man. J R Soc Med. 1993;86(5):287–289. doi: 10.1177/014107689308600515.
3. Wang Z-Y, Chen Z. Acute promyelocytic leukemia: from highly fatal to highly curable. Blood. 2008;111(5):2505–2515. doi: 10.1182/blood-2007-07-102798.
4. Sweeney CJ, Takimoto C, Wood L, et al. A pharmacokinetic and safety study of intravenous arsenic trioxide in adult cancer patients with renal impairment. Cancer Chemother Pharmacol. 2010;66(2):345–356. doi: 10.1007/s00280-009-1169-4.
5. Lu J, Chew E-H, Holmgren A. Targeting thioredoxin reductase is a basis for cancer therapy by arsenic trioxide. Proc Natl Acad Sci USA. 2007;104(30):12288–12293. doi: 10.1073/pnas.0701549104.
6. Miller WH, Schipper HM, Lee JS, et al. Mechanisms of action of arsenic trioxide. Cancer Res. 2002;62(14):3893–3903.
7. Shooshtary S, Behtash S, Nafisi S. Arsenic trioxide binding to serum proteins. J Photochem Photobiol B. 2015;148:31–36. doi: 10.1016/j.jphotobiol.2015.03.001.
8. Yu J, Qian H, Li Y, et al. Arsenic trioxide (As2O3) reduces the invasive and metastatic properties of cervical cancer cells *in vitro* and *in vivo*. Gynecol Oncol. 2007;106(2):400–406. doi: 10.1016/j.ygyno.2007.04.016.
9. Zhang J, Wang B. Arsenic trioxide (As2O3) inhibits peritoneal invasion of ovarian carcinoma cells *in vitro* and *in vivo*. Gynecol Oncol. 2006;103(1):199–206. doi: 10.1016/j.ygyno.2006.02.037.
10. Wang X, Li D, Ghali L, et al. Therapeutic potential of delivering arsenic trioxide into HPV-Infected cervical cancer cells using liposomal nanotechnology. Nanoscale Res Lett. 2016;11(1):94. doi: 10.1186/s11671-016-1307-y.
11. Song X, You J, Wang J, et al. Preparation and investigation of arsenic trioxide-loaded polylactic acid/magnetic hybrid nanoparticles. Chem Res Chin Univ. 2014;30(2):326–332. doi: 10.1007/s40242-014-3306-9.
12. Abbasi H, Rahbar N, Kouchak M, et al. Functionalized liposomes as drug nanocarriers for active targeted cancer therapy: a systematic review. J Liposome Res. 2022;32(2):195–210. doi: 10.1080/08982104.2021.1903035.
13. Greish K. Enhanced permeability and retention (EPR) effect for anticancer nanomedicine drug targeting. Methods Mol Biol. 2010;624:25–37.
14. Wu J. The enhanced permeability and retention (EPR) effect: the significance of the concept and methods to enhance its application. J Pers Med. 2021;11(8):771. doi: 10.3390/jpm11080771.
15. Pattni BS, Chupin VV, Torchilin VP. New developments in liposomal drug delivery. Chem Rev. 2015;115(19):10938–10966. doi: 10.1021/acs.chemrev.5b00046.
16. Li X, Wu X, Yang H, et al. A nuclear targeted dox-aptamer loaded liposome delivery platform for the circumvention of drug resistance in breast cancer. Biomed Pharmacother. 2019;117:109072. doi: 10.1016/j.biopha.2019.109072.
17. Nogueira E, Gomes AC, Preto A, et al. Design of liposomal formulations for cell targeting. Colloids Surf B Biointerfaces. 2015;136:514–526. doi: 10.1016/j.colsurfb.2015.09.034.
18. Khodarahmi M, Abbasi H, Kouchak M, et al. Nanoencapsulation of aptamer-functionalized 5-Fluorouracil liposomes using alginate/chitosan complex as a novel targeting strategy for Colon-specific drug delivery. J Drug Delivery Sci Technol. 2022;71:103299. doi: 10.1016/j.jddst.2022.103299.
19. Barbas A, Mi J, Clary B, et al. Aptamer applications for targeted cancer therapy. Future Oncol. 2010;6(7):1117–1126. doi: 10.2217/fon.10.67.
20. Javaherian S, Musheev MU, Kanoatov M, et al. Selection of aptamers for a protein target in cell lysate and their application to protein purification. Nucleic Acids Res. 2009;37(8):e62–e62. doi: 10.1093/nar/gkp176.
21. Strehlitz B, Nikolaus N, Stoltenburg R. Protein detection with aptamer biosensors. Sensors. 2008;8(7):4296–4307. doi: 10.3390/s8074296.
22. Tuerk C, Gold L. Systematic evolution of ligands by exponential enrichment: RNA ligands to bacteriophage T4 DNA polymerase. Science. 1990;249(4968):505–510. doi: 10.1126/science.2200121.
23. Ara MN, Matsuda T, Hyodo M, et al. Construction of an aptamer modified liposomal system targeted to tumor endothelial cells. Biol Pharm Bull. 2014;37(11):1742–1749. doi: 10.1248/bpb.b14-00338.
24. Mirveis Z, Kouchak M, Mahdavinia M, et al. Novel and efficient method for loading aptamer-conjugated liposomes with arsenic trioxide for targeting cancer cells. J Liposome Res. 2022;32(3):276–283. doi: 10.1080/08982104.2021.2005624.
25. Koutsioumpa M, Papadimitriou E. Cell surface nucleolin as a target for anti-cancer therapies. Recent Pat Anticancer Drug Discov. 2014;9(2):137–152. doi: 10.2174/1574892808666131119095953.
26. Krust B, El Khoury D, Nondier I, et al. Targeting surface nucleolin with multivalent HB-19 and related nucant pseudopeptides results in distinct inhibitory mechanisms depending on the malignant

tumor cell type. BMC Cancer,. 2011;11(1):333. doi: 10.1186/1471-2407-11-333.
27. Berger CM, Gaume X, Bouvet P. The roles of nucleolin subcellular localization in cancer. Biochimie. 2015;113:78–85. doi: 10.1016/j.biochi.2015.03.023.
28. Bates PJ, Laber DA, Miller DM, et al. Discovery and development of the G-rich oligonucleotide AS1411 as a novel treatment for cancer. Exp Mol Pathol. 2009;86(3):151–164. doi: 10.1016/j.yexmp.2009.01.004.
29. El Khoury D, Destouches D, Lengagne R, et al. Targeting surface nucleolin with a multivalent pseudopeptide delays development of spontaneous melanoma in RET transgenic mice. BMC Cancer,. 2010;10(1):325. doi: 10.1186/1471-2407-10-325.
30. Plourde K, Derbali RM, Desrosiers A, et al. Aptamer-based liposomes improve specific drug loading and release. J Control Release. 2017;251:82–91. doi: 10.1016/j.jconrel.2017.02.026.
31. Song XR, Zhang J, Wang G, et al. Targeted delivery of doxorubicin to breast cancer cells by aptamer functionalized DOTAP/DOPE liposomes. Oncol Rep. 2015;34(4):1953–1960. doi: 10.3892/or.2015.4136.
32. Xing HT, Yang X, Hwang K, et al. Selective delivery of an anticancer drug with aptamer-functionalized liposomes to breast cancer cells in vitro and in vivo. J Mater Chem B. 2013;1(39):5288–5297. doi: 10.1039/C3TB20412J.
33. Kouchak M. In situ gelling systems for drug delivery. Jundishapur J Nat Pharm Prod. 2014;9(3):e20126. doi: 10.17795/jjnpp-20126.
34. Ruel-Gariepy E, Leroux J-C. In situ-forming hydrogels—review of temperature-sensitive systems. Eur J Pharm Biopharm. 2004;58(2):409–426. doi: 10.1016/j.ejpb.2004.03.019.
35. Jeong B, Kim SW, Bae YH. Thermosensitive sol–gel reversible hydrogels. Adv Drug Delivery Rev. 2012;64:154–162. doi: 10.1016/j.addr.2012.09.012.
36. Dumortier G, Grossiord JL, Agnely F, et al. A review of poloxamer 407 pharmaceutical and pharmacological characteristics. Pharm Res. 2006;23(12):2709–2728. doi: 10.1007/s11095-006-9104-4.
37. Yuan Y, Cui Y, Zhang L, et al. Thermosensitive and mucoadhesive in situ gel based on poloxamer as new carrier for rectal administration of nimesulide. Int J Pharm. 2012;430(1–2):114–119. doi: 10.1016/j.ijpharm.2012.03.054.
38. Moghimipour E, Rezaei M, Ramezani Z, et al. Folic acid-modified liposomal drug delivery strategy for tumor targeting of 5-fluorouracil. Eur J Pharm Sci. 2018;114:166–174. doi: 10.1016/j.ejps.2017.12.011.
39. Ma Y, Zhang C, Chen X, et al. The influence of modified pluronic F127 copolymers with higher phase transition temperature on arsenic trioxide-releasing properties and toxicity in a subcutaneous model of rats. Aaps Pharmscitech. 2012;13(2):441–447. doi: 10.1208/s12249-012-9756-9.
40. Nie S, Hsiao WW, Pan W, et al. Thermoreversible pluronic® F127-based hydrogel containing liposomes for the controlled delivery of paclitaxel: in vitro drug release, cell cytotoxicity, and uptake studies. Int J Nanomedicine. 2011;6:151–166. doi: 10.2147/IJN.S15057.
41. Xu S, An X. Preparation, microstructure and function for injectable liposome-hydrogels. Colloids Surf, A. 2019;560:20–25. doi: 10.1016/j.colsurfa.2018.09.037.
42. Han S-M, Na Y-G, Lee H-S, et al. Improvement of cellular uptake of hydrophilic molecule, calcein, formulated by liposome. J Pharm Investig. 2018;48(5):595–601. doi: 10.1007/s40005-017-0358-0.
43. Cadinoiu AN, Rata DM, Atanase LI, et al. Aptamer-functionalized liposomes as a potential treatment for basal cell carcinoma. Polymers. 2019;11(9):1515. doi: 10.3390/polym11091515.
44. Taghavi S, Nia AH, Abnous K, et al. Polyethylenimine-functionalized carbon nanotubes tagged with AS1411 aptamer for combination gene and drug delivery into human gastric cancer cells. Int J Pharm. 2017;516(1–2):301–312. doi: 10.1016/j.ijpharm.2016.11.027.
45. Akhtar A, Wang SX, Ghali L, et al. Effective delivery of arsenic trioxide to HPV-positive cervical cancer cells using optimised liposomes: a size and charge study. Int J Mol Sci. 2018;19(4):1081. doi: 10.3390/ijms19041081.
46. Xu R, Song P, Wang J, et al. Bioleaching of realgar nanoparticles using the extremophilic bacterium *Acidithiobacillus ferrooxidans* DLC-5. Electron J Biotechnol. 2019;38:49–57. doi: 10.1016/j.ejbt.2019.01.001.
47. Micheletto YMS, Da Silveira NP, Barboza DM, et al. Investigation of self-association between new glycosurfactant N-acetyl-β-d-glucosaminyl-PEG-docosanate and soybean phosphatidylcholine into vesicles. Colloids Surf, A. 2015;467:166–172. doi: 10.1016/j.colsurfa.2014.11.052.
48. Xie J, Li Y, Song L, et al. Design of a novel curcumin-soybean phosphatidylcholine complex-based targeted drug delivery systems. Drug Deliv. 2017;24(1):707–719. doi: 10.1080/10717544.2017.1303855.
49. Wang S, Liu C, Wang C, et al. Arsenic trioxide encapsulated liposomes prepared via copper acetate gradient loading method and its antitumor efficiency. Asian J Pharm Sci. 2020;15(3):365–373. doi: 10.1016/j.ajps.2018.12.002.
50. Desai P, Jain N, Sharma R, et al. Effect of additives on the micellization of PEO/PPO/PEO block copolymer F127 in aqueous solution. Colloids Surf A. 2001;178(1–3):57–69. doi: 10.1016/S0927-7757(00)00493-3.
51. Matthew JE, Nazario YL, Roberts SC, et al. Effect of mammalian cell culture medium on the gelation properties of pluronic® F127. Biomaterials. 2002;23(23):4615–4619. doi: 10.1016/s0142-9612(02)00208-9.
52. Bonacucina G, Spina M, Misici-Falzi M, et al. Effect of hydroxypropyl β-cyclodextrin on the self-assembling and thermogelation properties of poloxamer 407. Eur J Pharm Sci. 2007;32(2):115–122. doi: 10.1016/j.ejps.2007.06.004.
53. Fakhari A, Corcoran M, Schwarz A. Thermogelling properties of purified poloxamer 407. Heliyon. 2017;3(8):e00390. doi: 10.1016/j.heliyon.2017.e00390.
54. Liu Y, Lu W-L, Wang J-C, et al. Controlled delivery of recombinant hirudin based on thermo-sensitive pluronic® F127 hydrogel for subcutaneous administration: *in vitro* and *in vivo* characterization. J Control Release. 2007;117(3):387–395. doi: 10.1016/j.jconrel.2006.11.024.
55. Sharma PK, Reilly MJ, Jones DN, et al. The effect of pharmaceuticals on the nanoscale structure of PEO–PPO–PEO micelles. Colloids Surf B Biointerfaces. 2008;61(1):53–60. doi: 10.1016/j.colsurfb.2007.07.002.
56. Liu B, Pan S, Dong X, et al. Opposing effects of arsenic trioxide on hepatocellular carcinomas in mice. Cancer Sci. 2006;97(7):675–681. doi: 10.1111/j.1349-7006.2006.00230.x.
57. Davison K, Mann KK, Miller WH. JrArsenic trioxide: mechanisms of action. Semin Hematol. 2002;39(2 Suppl 1):3–7. doi: 10.1053/shem.2002.33610.
58. Shen S, Lee J, Weinfeld M, et al. Attenuation of DNA damage-induced p53 expression by arsenic: a possible mechanism for arsenic co-carcinogenesis. Mol Carcinog. 2008;47(7):508–518. doi: 10.1002/mc.20406.
59. Wen G, Calaf GM, Partridge MA, et al. Neoplastic transformation of human small airway epithelial cells induced by arsenic. Mol Med. 2008;14(1-2):2–10. doi: 10.2119/2007-00090.Wen.
60. Yedjou C, Tchounwou P, Jenkins J, et al. Basic mechanisms of arsenic trioxide (ATO)-induced apoptosis in human leukemia (HL-60) cells. J Hematol Oncol. 2010;3(1):28. doi: 10.1186/1756-8722-3-28.
61. Li YM, Broome JD. Arsenic targets tubulins to induce apoptosis in myeloid leukemia cells. Cancer Res. 1999;59(4):776–780.
62. Zhang TD, Chen GQ, Wang ZG, et al. Arsenic trioxide, a therapeutic agent for APL. Oncogene. 2001;20(49):7146–7153. doi: 10.1038/sj.onc.1204762.
63. Chen MJ, Yang PY, Ye YZ, et al. Arsenic trioxide induces apoptosis in uveal melanoma cells through the mitochondrial pathway. Am J Chin Med. 2010;38(6):1131–1142. doi: 10.1142/S0192415X 10008524.

64. You BR, Park WH. Arsenic trioxide induces human pulmonary fibroblast cell death via increasing ROS levels and GSH depletion. Oncol Rep. 2012;28(2):749–757. doi: 10.3892/or.2012.1852.
65. Reyes-Reyes EM, Teng Y, Bates PJ. A new paradigm for aptamer therapeutic AS1411 action: Uptake by macropinocytosis and its stimulation by a nucleolin-dependent mechanism. Cancer Res. 2010;70(21):8617–8629. doi: 10.1158/0008-5472.CAN-10-0920.
66. Liao ZX, Chuang EY, Lin CC, et al. An AS1411 aptamer-conjugated liposomal system containing a bubble-generating agent for tumor-specific chemotherapy that overcomes multidrug resistance. J Control Release. 2015;208:42–51. doi: 10.1016/j.jconrel.2015.01.032.